International Journal of Greenhouse Gas Control 110 (2021) 103427

Contents lists available at ScienceDirect

International Journal of Greenhouse Gas Control

journal homepage: www.elsevier.com/locate/ijggc

Quantification of a subsea CO_2 release with lab-on-chip sensors measuring benthic gradients

Allison Schaap [a,*], Dirk Koopmans [b], Moritz Holtappels [c], Marius Dewar [d], Martin Arundell [a], Stathys Papadimitriou [a], Rudolf Hanz [a], Samuel Monk [a,e], Matthew Mowlem [a,e], Socratis Loucaides [a]

[a] National Oceanography Centre, Waterfront Campus, European Way, Southampton SO14 3ZH, UK
[b] Max Planck Institute for Marine Microbiology, Celsiusstr. 1, D-28359, Bremen, Germany
[c] Alfred Wegener Institute for Polar and Marine Research, Postfach 12 01 60, 27515, Bremerhaven, Germany
[d] Plymouth Marine Laboratory, Prospect Pl., Plymouth PL1 3DH, UK
[e] Presently also at ClearWater Sensors Ltd., UK

ARTICLE INFO

Keywords:
Carbon capture and storage
Reservoir monitoring
Autonomous sensors
Benthic gradients
Plume quantification

ABSTRACT

We present a novel approach to detecting and quantifying a subsea release of CO_2 from within North Sea sediments, which mimicked a leak from a subsea CO_2 reservoir. Autonomous lab-on-chip sensors performed in situ measurements of pH at two heights above the seafloor. During the 11 day experiment the rate of CO_2 release was gradually increased. Whenever the currents carried the CO_2-enriched water towards the sensors, the sensors measured a decrease in pH, with a strong vertical gradient within a metre of the seafloor. At the highest release rate, a decrease of over 0.6 pH units was observed 17 cm above the seafloor compared to background measurements. The sensor data was combined with hydrodynamic measurements to quantify the amount of CO_2 escaping the sediments using an advective mass transport model. On average, we directly detected 43 ± 8% of the released CO_2 in the water column. Accounting for the incomplete carbonate equilibration process increases this estimate to up to 61 ± 10%. This technique can provide long-term in situ monitoring of offshore CO_2 reservoirs and hence provides a tool to support climate change mitigation activities. It could also be applied to characterising plumes and quantifying other natural or anthropogenic fluxes of dissolved solutes.

1. Introduction

Atmospheric carbon dioxide concentration has risen to >407 parts per million, a 47% increase over the concentration at the beginning of the industrial era (Friedlingstein et al., 2019). Carbon capture and storage (CCS) has been proposed as a tool to decrease emissions or atmospheric concentrations of CO_2; this approach is included in many mitigation scenarios for keeping global warming to below 1.5 °C above pre-industrial levels (IPCC, 2005; Gale et al., 2015, 2018)). In Europe, most of the identified CO_2 storage capacity is in offshore sites, including in depleted subsea oil and gas reservoirs (IEA Greenhouse Gas R&D Programme (IEA GHG) 2008). A requirement for this offshore CO_2 storage is the ability to monitor and ensure reservoir integrity during and after the initial storage activity (Dean et al., 2020). This is necessary to satisfy regulatory requirements and to alleviate public concern around potential risks (Mabon et al., 2015). Reservoir integrity can be monitored in the reservoir itself but must also be complemented by monitoring for emissions of CO_2 into the overlying seawater (Dean and Tucker, 2017). Any techniques used to monitor for emissions should be sufficiently sensitive that the emission is detected and quantified before the regulatory limit is breached, and before any damage can occur to the local environment or ecosystem. Such monitoring techniques need to be developed and validated at low, known rates of CO_2 release in a relevant environment, to provide confidence in their suitability.

To this end, various novel methods for detecting a small subsea release CO_2 were developed and demonstrated in the context of the EU project "STEMM-CCS" (Strategies for environmental monitoring of marine carbon capture and storage; see (Flohr et al., 2021b)). Custom-built equipment enabled a release of CO_2 at a controllable flow rate 3 m below the seafloor, designed to mimic a leak from an offshore storage facility.

Here we present a novel approach to detecting and quantifying this CO_2 release in the water column using novel autonomous sensors

* Corresponding author.
E-mail address: allison.schaap@noc.ac.uk (A. Schaap).

https://doi.org/10.1016/j.ijggc.2021.103427
Received 17 December 2020; Received in revised form 24 June 2021; Accepted 3 August 2021
Available online 17 August 2021

measuring parameters of the carbonate system in seawater. The instruments, mounted on a seafloor lander, sampled at two altitudes above the seafloor. This data, combined with information about the local hydrodynamics, allowed for detection and quantification of the CO_2 release.

The technique described here is inspired by the gradient flux approach for quantifying vertical fluxes of solutes in the benthic boundary layer. In this approach, the concentration of a solute is measured at multiple vertical distances from the seafloor and coupled with measurements or estimates of local hydrodynamic properties. This technique has been used for the measurement of oxygen and indirectly for nutrients through the collection and subsequent analysis of samples (Holtappels et al., 2011), and for the measurement of oxygen (McGillis et al., 2011) and oxygen and pH (Takeshita et al., 2016) fluxes in a coral reef using autonomous in situ sensors.

Here, we use a set up adapted from the gradient flux setup to quantify a mass flow of CO_2 from a point on the seafloor. The source of the signal of interest (dissolved inorganic carbon) is not a planar vertical flux from the seafloor, but instead is the result of the turbulent advection of a vertical line source with a strong concentration gradient. As the CO_2 escapes from the sediment into the overlying water column it is typically in the form of a stream of gaseous bubbles. These bubbles readily dissolve in seawater and together with dissolved CO_2 emissions from the sediment, form strong pH and dissolved inorganic carbon (DIC) gradients towards the seabed. Measurements of pH and alkalinity are used to calculate the excess DIC in the water column from the CO_2 release, and coupled to an advective mass transport model based on measurements of current to estimate total excess DIC mass flow.

To detect this source of CO_2 we use lab-on-chip (LOC) sensors. These devices implement standard laboratory assays in situ on a miniaturized, automated hardware platform. To measure the CO_2 release, we developed and deployed sensors to measure pH and total alkalinity (TA). These were deployed on landers near the release point, along with LOC sensors for nitrate and phosphate, to perform contextual measurements for stoichiometric analysis (Omar et al., 2021).

Throughout the CO_2 release experiment, other equipment for the detection, characterisation, and quantification of the gaseous and dissolved CO_2 were also deployed around the site (Flohr et al., 2021b). This included the deployment of additional LOC sensors (pH, TA, nutrients) and other pH sensors on an ROV (Monk et al., 2021). Other tools for measuring benthic fluxes were also applied to detect and quantify the CO_2 release. Benthic chambers directly measured fluxes at the sediment-water interface by monitoring solute concentration within an enclosed volume of water (Connelly, 2019). pH eddy covariance measured the turbulence-driven vertical fluxes of hydrogen ions from the dissolved CO_2 through high frequency measurements of pH and eddy velocities at a single point above the seafloor (Connelly, 2019; Koopmans et al., 2021). Other techniques included optical and acoustic measurements along with direct sample collection. An overview of these can be found elsewhere in this special issue (Flohr et al., 2021b).

2. Material and methods

2.1. Experimental site and CO_2 release

The CO_2 release equipment and technologies for detection and quantification of the release were deployed in a field experiment in the North Sea in May 2019 (Connelly, 2019; Flohr et al., 2021b). The field site was located at a depleted oil and gas reservoir, the Goldeneye complex (58° 0′ 10.8″ N, 0° 22′ 48″ W, approx. 100 km off the coast of Scotland), which has been identified as a potential offshore CO_2 storage facility. The site has 120 m water depth. The currents in the region are driven by a tidal cycle with a period of ~12.5 h; they are predominantly north-south and rotate counter-clockwise along an ellipsoidal path.

The CO_2 was released within the sediments, 3 m below the seafloor, via a pipe and hose system connected to the CO_2 storage and release system located 80 m away (Fig. 1c). Details of the equipment can be found elsewhere (Flohr et al., 2021b). The release began at a flow rate of 6 kg/d during Day 0 of the experiment (11 May 2019). Streams of CO_2 bubbles were seen emitting steadily from the sediment within the 30 min it took the ROV to move from the gas control unit to the bubble emission area. The flow rate was increased step-wise over 11 days, culminating in a maximum release rate of 143 kg/d. During this time additional bubble streams emerged within a 2 m radius of the experimental epicentre, with most of them roughly along the east-west axis of this point. The release rates were chosen to cover a large range of rates below the estimated maximum permissible leakage rate of a CCS facility at this site, 274 kg/d (Flohr et al., 2021b). These rates also envelop the 8–150 kg/d range of leakage that can occur along the outside of wells due to sediment fractures caused by drilling (Vielstädte et al., 2019).

Throughout the experiment, other equipment for the detection, characterisation, and quantification of the gaseous and dissolved CO_2 through other means were also deployed around the site, including the deployment of LOC sensors on an ROV (Monk et al., 2020). Direct sampling was complemented by other in situ chemical, optical, and acoustic measurement in the sediment and the water column; an overview of the techniques can be found elsewhere (Flohr et al., 2021b).

2.2. Sensors and instrumentation

The measurements used in the CO_2 detection and quantification approach described in this paper were performed by LOC sensors which use a common hardware platform for implementing chemical assays (Beaton et al., 2012). These sensors are based around microfluidic chips: plastic discs with micro-scale channels and recesses machined onto their surfaces (Fig. 1a). These are bonded together to form a network of fluidic ports and channels. Some of these channels form optical cells in which optical absorbance measurements are performed. Pumps, valves, and electronics are mounted directly onto the chips (Fig. 1a), and the whole assembly is placed in a waterproof pressure-compensating housing. Reagents and (where applicable) calibration standards are stored in flexible bags external to the housing. Reagents and samples are pumped into the device with a deep-sea compatible syringe pump and valves. The sample and reagents mix in the fluidic channels and the reaction products are analysed optically.

The pH sensor utilises the standard seawater spectrophotometric pH method using purified meta-Cresol Purple indicator dye (Dickson et al., 2007). The sensor is described elsewhere (Rérolle et al., 2013; Yin et al., 2021) but in brief: a small plug of dye is introduced into a long (80 cm) channel full of seawater sample. As the dye plug moves along the channel, an axial dispersion curve of dye is created as a function of distance and hence time at a fixed location. This dye passes through an optical cell at the end of the channel where the sample is illuminated by two LEDs (peak wavelengths 435 and 590 nm) and the intensity of the transmitted light is measured with a photodiode. The optical absorbance of the sample is calculated from the Beer-Lambert law, referenced to the intensity measured while the blank seawater (without dye) passed through the cell directly ahead of the dye. This compensates for any intrinsic light absorptivity of the sample and any slow-scale optical drift caused by channel staining or changes in LED output levels. From this measurement the pH of the dye-free seawater is calculated. Because the peak wavelength of the 590 nm LED is further away than the absorbence maximum wavelength of mCP (578 nm), the sensor is calibrated along a 0 - 40 °C temperature gradient with in-house, gravimetrically prepared Tris–HCl synthetic seawater ($S = 35$) buffers against their historical temperature-dependant (at constant $S = 35$) pH value determined in the Harned cell by DelValls and Dickson (1998). The pH sensor was validated for its conformity with the spectrophotometric method on the benchtop Cary UV–Vis 600 spectrophotometer using validation seawater samples under laboratory-controlled conditions and in the field, and the overall measurement uncertainty of the sensor has been estimated at ≤0.010 pH units at pH = 8 and ≤0.014 pH units at pH =

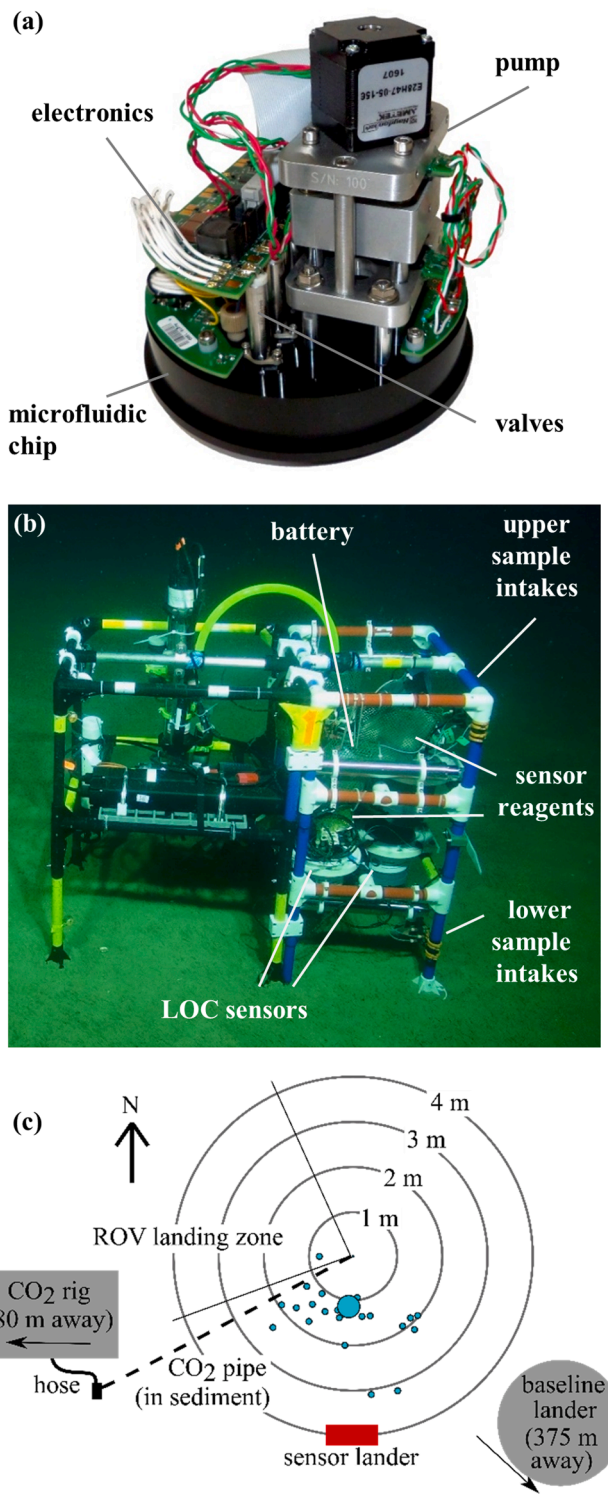

Fig. 1. (a) Lab-on-chip sensor out of its housing, showing the microfluidic chip, fluidic components, and electronics for control, power, and communications. (b) Lander and sensors with an upper and lower intake for each sensor. Bags of sensor reagents or standards fixed to the lander frame. (c) Top-down view of the layout of the experimental site, showing the sensor lander in red, the bubble positions as small dots with the bubble epicentre as one large blue dot, the CO_2 release equipment and baseline lander. The plot epicentre is the expected location of the end of the CO_2 pipe, which had a 46 cm long diffuser at the release end. (For interpretation of the references to colour in this figure legend, the reader is referred to the web version of this article.)

7.5. Further information on the sensor can be found in Yin et al. (2021). The entire measurement cycle takes approximately 10 min, with 5.7 min of flushing, 0.5 min of sample collection from the surrounding environment, and 3.5 min of injecting and analysing the sample pH. Each measurement is timestamped to the middle of the sample collection step.

The TA sensor implements a single-step open-cell titration (Breland and Byrne, 1993; Li et al., 2013) where seawater is mixed with a salinity-matched titrant comprising hydrochloric acid, bromophenol blue pH indicator, and a surfactant (Tween-20). The CO_2 produced is removed into NaOH in a gas exchange column. The mixed, degassed solution enters an optical cell where its optical absorbance is measured at two wavelengths (435 nm and 591 nm). This yields the pH of the mixed, degassed solution which allows calculation of the TA of the seawater sample (overview available in (Wang et al., 2019)). The sensor carries two certified reference materials for re-calibration in the field. The materials (CO_2 Seawater Reference Materials, Scripps Institute of Oceanography, batches 162 and 180) are re-measured after each 20 samples and used by the instrument to provide environmentally-dependant calibration terms in the TA calculation. The overall measurement uncertainty of this sensor in temperature-stable field deployments has been estimated at ± 5 μmol/kg and each measurement takes 10 min.

The LOC sensors were mounted onto custom-built landers (Fig. 1b). Each lander had a LOC sensor for pH and TA, along with additional sensors and equipment. Each LOC sensor had two inlets, each with an 80 cm long sampling tube and a 0.45 μm pore size PES syringe filter at the intake end of the sampling tube. One intake filter for each sensor was placed near the bottom of the frame (16.9 ± 2.2 cm from the seabed) and one near the top of the frame (87.2 ± 2.2 cm above the seabed). The sensors alternated between taking samples from the two inlets. The goal of this approach was to characterize the vertical concentration gradient in each parameter, if any, and to use this to quantify the total CO_2 emission from the seafloor by the release experiment.

The same landers also housed a pH eddy covariance system (Koopmans et al., 2021). This system included a water velocimeter (Nortek Vector, Nortek AS, Norway) which performed high frequency measurements (>1 Hz) at 16 cm above the seafloor. On separate lander 375 m to the southeast, a single-point current metre (Nortek Aquadopp 3000 m, Nortek AS, Norway) measured the current every 10 min at 1.2 m height (Fig. 2a). Data from these two instruments was used to estimate the current velocity profile near the seabed.

The landers were deployed by remote-operated vehicle (ROV) and positioned 2.6 m due south of the bubble stream epicentre (Fig. 1c). The ROV had an equipment weight limit which prohibited the landers from holding enough batteries to run all of the systems continuously throughout the experiment. Instead, two identical landers were prepared, each with enough batteries to operate continuously for 48 h. Each LOC sensor was powered by a set of 4 D cell batteries in a deep-sea-rated titanium housing. The landers were swapped at the seafloor by the ROV every 48 h to allow for continuous monitoring of the CO_2 signal before, during, and after the release.

2.3. *Quantification of the CO_2*

Quantifying the CO_2 in the water column requires knowledge of the concentration and spatial distribution of the CO_2. Rather than measure a quasi-steady-state plume with a spatially-distributed array of sensors, we use a single sensor in a fixed location and rely on the counter clockwise progression of the tidal ellipse to sweep the entire plume of CO_2-enriched waters over the sensors during each tidal cycle. To optimize this approach, the lander is positioned so that it is exposed to the plume over much of the tidal cycle (Fig. 2a).

The pH time series data from the sensors was used to calculate a time series of excess DIC (Fig. 2b) using the software package CO_2SYS (Lewis and Wallace, 1998; van Heuven et al., 2011); the carbonic acid dissociation constants used were the recommended pairing ((Mehrbach et al.,

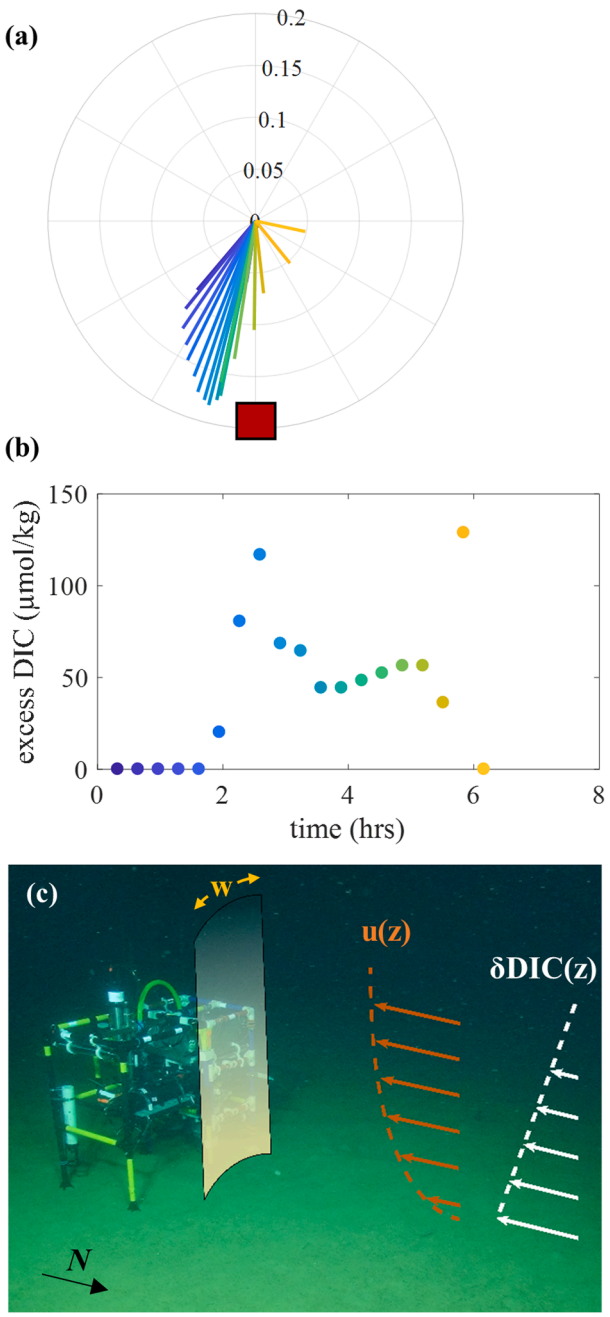

Fig. 2. (a) Plot of the near-southbound currents during one tidal cycle; the length of the line is the current speed in m/s (scale indicated on the top). The red box indicates the position of the lander relative to the cardinal directions and the black dashed line is the range of directions over which the plume was detected. (b) The excess DIC at 16 cm altitude, calculated at the same time points, with the colours matching those of the simultaneously measured currents in (a). (c) Illustration of the system geometry and of the terms u(z), δDIC (z), and w. The lander is due south of the bubble streams. The currents sweep the plume of excess DIC over the lander. The total DIC content of the plume is calculated for each segment of data by integrating the flux over a surface with arc width w. (For interpretation of the references to colour in this figure legend, the reader is referred to the web version of this article.)

1973) refit by (Dickson and Millero, 1987)) as were the KSO_4 dissociation constants (Dickson, 1990) and the oceanic concentration of total boron (Uppström, 1974)). Since there was no pattern observed in temperature (T), or salinity (S) with currents, time of day, or height from the seafloor, the average values of these parameters were used. Their means ± 1 σ were $T = 7.71 \pm 0.047$ °C, $S = 35.10 \pm 0.033$, TA = 2310.6 ± 26.6 µmol/kg (based on bottle sampling), phosphate = 0.61 ± 0.10 µM. The time series data was split into 20-minute segments with each segment containing two lab-on-chip pH readings, one from each inlet, with five minutes on either side.

We calculate the total excess DIC of each segment (DIC_n) as

$$DIC_n = \int_{seafloor}^{open\ water} w_n * \delta DIC_n(z) * u_n(z)\ dz \quad (1)$$

where w_n is the horizontal arc length of each segment, $\delta DIC_n(z)$ is the vertical concentration distribution of excess DIC, $u_n(z)$ the vertical profile of the current magnitude, and z the vertical variable (Fig. 2c).

The total DIC content of the plume entering the water column, measured over one tidal cycle, is the sum of the DIC mass flow rates in each segment within a single tidal cycle:

$$DIC_{plume} = \sum_n DIC_n \quad (2)$$

Each of the factors in the terms of Eq. (1) can be calculated using physical models parameterized by experimental data, as follows; illustrations can be seen in Fig. 2c.

The arc length w_n of each measured segment of plume is derived from current geometry

$$w_n = L\ \theta \quad (3)$$

where L is the distance between the lander and the epicentre of the bubble ebullition points, and θ the change in current direction between the start and end of the segment, in radians.

The excess DIC distribution, $\delta DIC_n(z)$, is estimated from a bubble dissolution model (Dewar et al., 2021, 2015). The bubbles were not fully dissolved until they were several metres above the seafloor. By scaling the outcomes of the model to the measurements of the excess DIC in the water column at two heights above the seafloor we can represent the full vertical distribution of DIC in the water column at the sensor location:

$$\delta DIC_n(z) = r_n \frac{(a + b\ e^{-cz})}{u_n(z)} \quad (4)$$

The values of the dimensionless constants a, b, and c were defined by an exponential approximation of the bubble dissolution model output. The bubble dissolution model assumes an average bubble diameter of 4 mm, with $a = -0.936$, $b = 2.385$ and $c = 0.450$. This diameter was based on estimates of bubble size made from in situ optical and acoustic measurements (Li et al., 2021) which showed a modal bubble diameter of 3.4 mm and a median bubble diameter of 5.3 mm. The constant r_n is the scaling term (in $mol/m^3/s$) to match the model to the data and is calculated from a least-squares fit of the model to three δDIC concentrations: one at the lower sensor inlet, one at the higher sensor inlet, and one in the overlying water column where δDIC = 0. $\delta DIC_n(z)$ thus describes the height-dependant bubble dissolution, diluted in the plane perpendicular to the sediments by the current velocity at each height z, and scaled to the observed levels of excess DIC. The emission of excess DIC from the sediment pore water was neglected as experimental results showed that it was negligible (Lichtschlag et al., 2020). After the rate constant was determined for each segment, the residuals of the fitted $\delta DIC_n(z)$ vs z curve were calculated for each integer mm bubble diameter. The fits to the 4 mm diameter bubbles had the lowest residuals which confirmed that this bubble size was the most appropriate to use.

To estimate the current velocity $u_n(z)$ during each segment we use the log-law velocity profile

$$u_n(z) = \frac{u_*}{\kappa} \ln\left(\frac{z}{z_o}\right) \quad (5)$$

where z_o is the bottom roughness, u_* is the velocity-dependant friction velocity, κ is von Kármán's constant ($k = 0.41$). z_0 was held constant

while u_* was scaled to meet the observed velocity gradient.

The physical constants u_* and z_o were estimated by using values of $u_n(z)$ at two heights z_1 and z_2 from the two current sensors to simultaneously solve for

$$z_o = \exp\left(\frac{u(z_1)\ln(z_2) - u(z_2)\ln(z_1)}{u(z_1) - u(z_2)}\right) \quad (6)$$

$$u_* = \frac{u(z_1)k}{\ln\left(\frac{z_1}{z_o}\right)} \quad (7)$$

The product of $u_n(z)$ and $\delta DIC(z)$ yields a flux over the surface at radius 2.6 m from the bubble source. The total excess DIC mass flow rate in each segment DIC_n is calculated by multiplying this flux by the arc length of each segment (w_n) and integrating over the vertical term z from the seafloor to the open water column (see illustration, Fig. 2c).

3. Results

3.1. Background measurements: hydrodynamics and total alkalinity

The currents at the site oscillated between predominantly northbound and southbound (Fig. 4). The maximum flow speed was between 0.1 and 0.2 m/s. To provide representative values, during mean steady-state southbound currents, Eqs. (6) and 7 yielded values of $z_o = 2 \times 10^{-4}$ m and $u_* = 0.0073$ m/s.

The TA LOC sensors returned values of 2312.3 ± 25.5 μmol/kg at the upper inlet and 2308.9 ± 27.6 μmol/kg at the lower inlet (n = 562 samples at each inlet). There were no detectable correlations between TA and current direction, current magnitude, or time of day. Bottle samples were collected by a ship in the vicinity and subsequently analysed in a lab with standard methods (Esposito et al., 2020; Schmidt, 2019). Samples taken at depths >100 m showed TA=2319.8 ± 10.6 (n = 71 samples). Since the TA LOC sensors, which were experimental prototypes, showed low accuracy and high variability compared to the bottle samples, and since the TA sensor means and variance were not correlated to current direction (i.e. not affected by site activity or CO_2 release) or to time of day or height from the seafloor, the mean bottle sample TA values were used in calculations of the DIC concentration. More details on this point can be found in the Discussion section.

3.2. pH measurements

The pH LOC sensors took one measurement every 10 min. One sensor failed, causing the loss of data during one 48-hour deployment; it was replaced immediately afterwards with a backup sensor.

Before the CO_2 release began, the baseline pH ranged from 8.035 – 8.049 and showed small variations with current magnitude, with a small drop in pH (~10 mpH) during periods of high currents, whether north or southbound (Fig. 3) due to increased turbulent mixing (Holtappels et al., 2011). During this baseline period the difference between the upper and lower inlet never exceeded 5 mpH and the mean difference between them was 1.9 mpH.

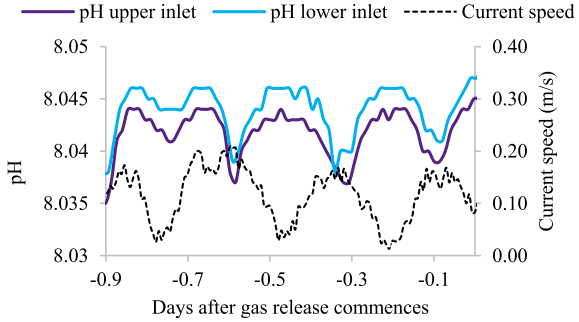

Fig. 3. Baseline pH measurements immediately before the CO_2 release.

As the CO_2 release rate increased, increasingly large drops in pH were detected in the water whenever the currents turned southwards (Fig. 4). Transient drops of >0.6 pH units (equivalent to a DIC increase of >200 μmol/kg) were detected at the lower sensor inlet during the highest CO_2 release rate.

There was a large difference between the upper and lower sensor intakes, with a notably lower pH at the lower inlet. During southbound currents at the highest release rate, the average pH at the lower and upper inlets was 7.85 and 7.98 respectively, equivalent to an excess DIC of 75 and 28 μmol/kg. Transient differences of >0.5 pH units between inlets were observed multiple times during this release rate.

The total DIC in the water column increases with CO_2 release rate but also varies within each release rate (Fig. 5). On average, 43 ± 8% (mean ± 1σ) of the CO_2 released by the CO_2 injection system was detected as DIC in the water column by this method. At the lowest release rate, small drops in pH were visible on both inlets of the sensors but only for one or two data points during near-stagnant flow conditions, when the excess DIC was building up in the volume of water directly around the bubble streams.

Uncertainties in DIC emission (the error bars on Fig. 5) include contributions due to a ± 0.5 mm uncertainty on bubble diameter and an estimated ± 0.005 pH unit uncertainty of the pH sensor. The uncertainty in TA had little effect as the CO_2 release quantification was a function of excess DIC rather than absolute DIC, and so was neglected here. However, our experimental setup has additional uncertainties which are more difficult to estimate. The bubble streams were intermittent and changed throughout the experiment; as a result, and because the DIC source was streams of individual bubbles in a moving current, the pH of the water at the lander was spatially inhomogeneous and changed rapidly (see data in (Koopmans et al., 2020) where pH data is collected at >1 Hz). The LOC sensors only measure one point every 10 min, resulting in undersampling relative to the timescales during which the pH of water in the plume of the bubble streams could change. Nevertheless, this measurement period is very fast compared to the 12.5 h tidal cycle and the ~4.5 h long period during which currents were within 45° of southbound during each tidal cycle.

4. Discussion

4.1. CO_2 quantification and relevance for CCS monitoring

The CO_2 release was successfully quantified using Eq. (2) at CO_2 release rates ≥14.3 kg/d. Regulations on maximum permitted leaks have not yet been established for offshore CCS. However, one can apply proposed limits to the planned injection rates for the reservoir above which this experiment took place (i.e. <0.001%/yr of 10 Mt). This yields a representative maximum leakage rate of 274 kg/d (Flohr et al., 2021b). This is nearly twenty times higher than the rate at which we demonstrated detection and quantification of the released CO_2.

The technique presented here likely underestimated the DIC in the water column due to the equilibration time of the carbonate system in seawater. Carbonate equilibration is a complex process with many variables, but for representative conditions of this experiment, the T90 (the time to get to 90% of the final equilibrium) is ~300 s (Koopmans et al., 2021; Schulz et al., 2006). Under steady-state southbound currents (~10–20 cm/s) the elapsed time between a volume of water passing through the bubble streams and being analysed in the LOC sensor's optical cell would have been between 160 and 175 s. With this elapsed time, only about 70% of the true signal would have been measured. Taking this into account increases the estimate of the CO_2 in the water column from 43 ± 8% to up to 61 ± 10% of that injected. This result was comparable with the estimates from other techniques used in the same experiment: at the highest release rate, the eddy covariance-based method measured 74% of the injected CO_2 in the

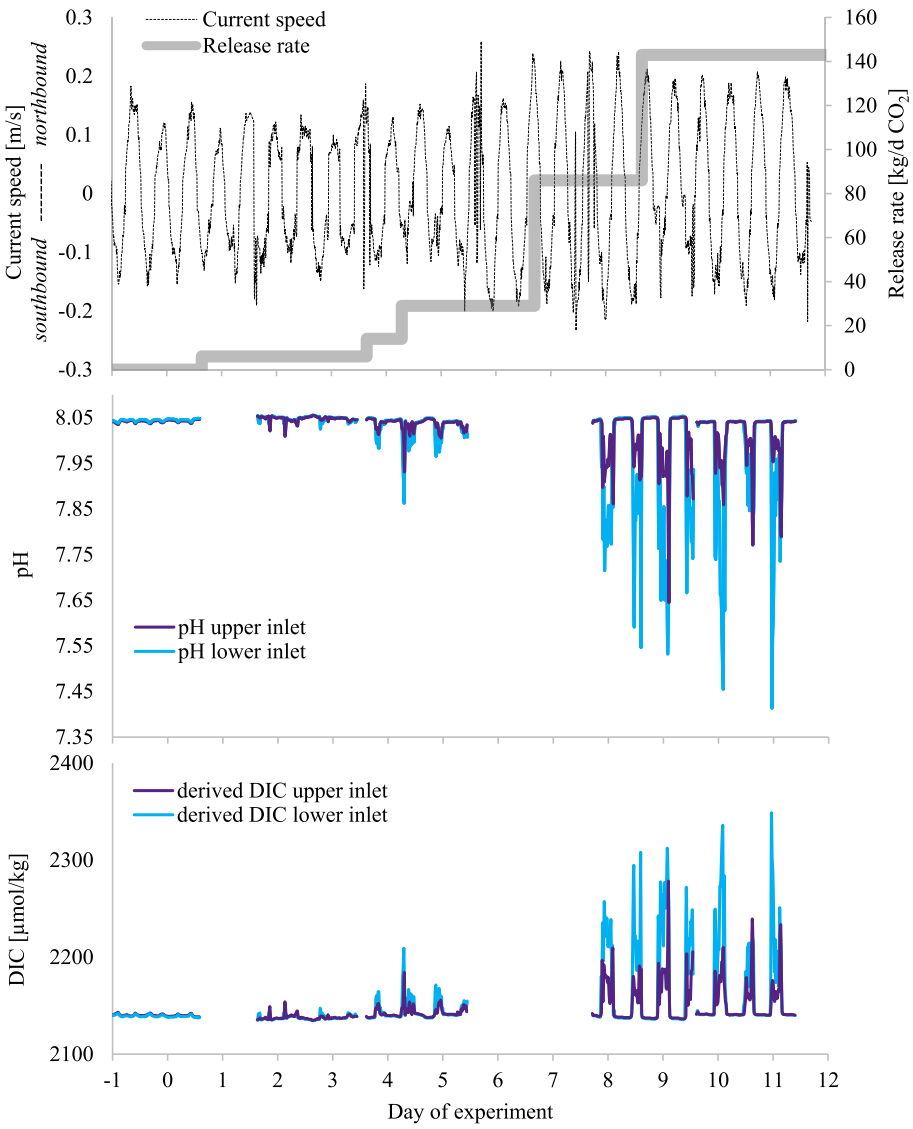

Fig. 4. Currents, CO_2 release rate, pH, and derived DIC time series throughout the field experiment. The current data is from the current meter on the eddy covariance system, and was measuring 16 cm above the seafloor. On this graph, negative speeds indicate currents with a southbound component and positive speeds northbound. For pH and derived DIC, data from the top sample inlet (dark purple) and bottom sample inlet (blue) of the sensor are shown. Note that the pH and DIC data are scaled to the left axis for days 1–6 and right axis for days 7–12 to show the full range of measurements. The period of missing data in days 5–7 is due to a failure of the pH sensor deployed during this 48 hour window. (For interpretation of the references to colour in this figure legend, the reader is referred to the web version of this article.)

water column on average (Koopmans et al., 2021), an ROV survey using pH sensors measured 57% (Monk et al., 2021), and a gas-collection method measured 48% (Flohr et al., 2021a). The remaining CO_2 is expected to have remained in the sediments, where evidence of both dissolved (de Beer et al., 2021; Lichtschlag et al., 2020) and gaseous (Roche et al., 2021) CO_2 was observed during the experiment. It is possible that the quantification was also underestimated by only including measurements from when the currents were within ± 45° of southbound. This cut-off was used to exclude CO_2 that accumulated in the water column at slack currents.

The amount of excess DIC measured in the water column varied within each injection rate. This may reflect several aspects of the variability of the experiment. The visible emission of CO_2 from the sediment was not steady: throughout the 11 day experiment, 22 different bubble streams were identified, starting and (in some cases) stopping at various injection rates. Some CO_2 may have been diverted to new streams (either included in or excluded from detection by the sensors, depending on location) throughout the course of a tidal cycle measurement period. The rate of retention of CO_2 within the sediment may have been inconsistent, either as rapid dissolution took place around newly-formed fractures or as pools of CO_2 formed within the sediment (Roche et al., 2021). In other experiments designed to mimic a seafloor CCS CO_2 leak, the presence and intensity of bubble plumes was affected by water depth (Kita et al., 2015), with higher release during lower tides. As all of the measurements taken here were during southbound currents, when the water depth was lower than during northbound currents, it is possible that this technique slightly overestimates the rate of CO_2 emission into the water column over an entire tidal cycle. However, the change in water depth due to tides here was at most ± 0.9% of the mean water depth so it is unlikely that this caused a significant effect.

The results of these measurements can inform the requirements for CCS monitoring techniques. The strong vertical gradient caused by the rapid dissolution of gaseous CO_2 in the water column means that it is important to measure near the seabed. The parameterised model of the DIC distribution suggests that the plume's signal would be virtually undetectable over 2 m height above the seabed. This conclusion is corroborated by results from other approaches to map the plume (Monk et al., 2021) and by pre-experiment models (Blackford et al., 2020). This outcome imposes strict conditions on the design of CCS monitoring approaches in areas with similar hydrodynamic and physical characteristics to our field site. Monitoring an entire reservoir requires large spatial coverage, which would ideally be achieved through putting sensors on an underwater vehicle rather than through a large array of fixed equipment. However, the strongest signals are found closest to the seabed, which is challenging location for operation of an autonomous underwater vehicle. It may be possible, or even necessary, for a vehicle

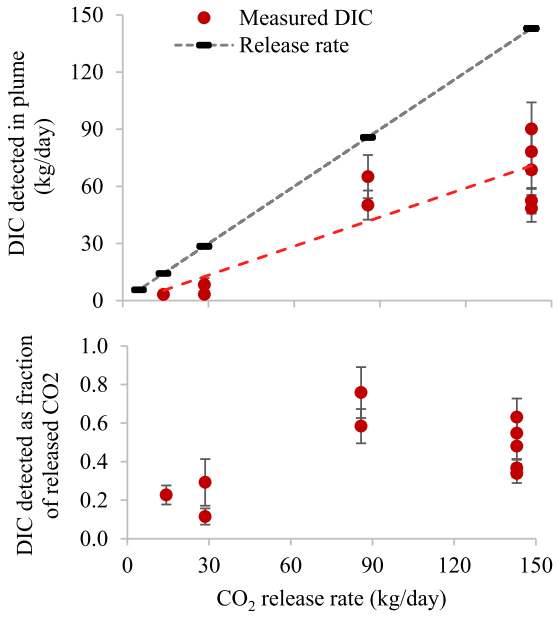

Fig. 5. DIC detected in the plume by the lab-on-chip based gradient flux system, compared to the rate of release of the CO_2.

to sample from a position below its main body, for example, by pumping sample water up from a weighted sample tube closer to the seafloor. This could be complemented by landers or moving benthic vehicles placed in or near strategic locations where a leak is more likely to occur – at a wellbore, for example (Dean and Tucker, 2017).

Previous work has suggested that, in a CCS context, a 0.1 decrease in pH would be a representative threshold beyond which some environmental impacts may be expected (Blackford et al., 2020). This value is smaller than the variation which can be observed in marine systems due to naturally-occurring seasonal cycles and is the estimated reduction in average surface seawater pH caused by human activities (Royal Society, 2005). To contextualize our measurements with this value, we observe that in our data from release rates of $\leq$29 kg/d, this threshold was only exceeded once. At the next-highest release rate (86 kg/d), the pH signal during southbound currents was, on average, 0.172 and 0.060 units lower than during the northbound currents at the lower and upper inlets, respectively and at the highest rate of 143 kg/d these values were 0.212 and 0.075. This technique was able to detect and quantify the CO_2 release at flow rates below those which would cause a 0.1 pH decrease even over a spatial area of square metres. Further sensitivity can be achieved by taking natural temporal and seasonal variability and stoichiometric ratios into account (Blackford et al., 2017). This approach has been demonstrated for the field experiment described here, using this data and others, and can be found elsewhere in this special issue (Omar et al., 2021).

4.2. Evaluation of this approach

The direct measurement of pH in seawater has benefits as a CCS monitoring approach. Proposed environmental impact thresholds have been expressed as a change in pH, so this measurement directly relates to the potential impact of a leak (Blackford et al., 2020). It could be paired with a complementary approach which has better coverage but lower specificity. For example, sonar-based detection of gas bubbles can examine a large area rapidly but cannot differentiate a CO_2 leak from a natural methane seep. For a more comprehensive comparison of the strengths and weaknesses of the full range of techniques and tools tested in this field experiment, the reader is referred to the "Monitoring and Decision Tool" prepared by the STEMM-CCS project (http://stemm-ccs.eu/monitoring-tool/) and the associated publication (Lichtschlag et al., 2021).

LOC sensors had some strengths compared to commercially-available pH sensors in this context. One notable advantage is the use of multiple inlets on a single sensor. This avoids the need for a separate pumping system to bring water from a variety of heights to a single device, simplifying the hardware requirements, reducing power consumption, and avoiding potential issues with equipment synchronisation, calibration and flushing times. The LOC sensors demonstrated here each had two inlets but could readily be modified to have more sample inlets, enabling a higher spatial resolution. All of these sensors use spectrophotometric analyses for measurements and can carry preserved standards for re-calibration in the field. This provides a high performance standard over a long-term deployment, an important consideration for a longer-term offshore CCS monitoring scenario.

However, these sensors also have disadvantages compared to some commercial technology. Wet chemical analysis has an inherently slower response time compared to purely optical or electrochemical methods. For example, a SeaFET (Sea-Bird Scientific, USA) can provide pH data at 1 Hz. pH optodes, which were deployed on an ROV in the same field experiment, provided data at higher speeds albeit with a system response time of ~3 min (Monk et al., 2021; Staudinger et al., 2018). The LOC pH sensor could analyse one sample every 10 min. In the present work this was not a major constraint, as the low-pH plume lasted for 4.5–5 h. In an arbitrary monitoring scenario the duration of the signal may be shorter, depending on the CO_2 leak rate and the relative position of the lander, the leak, and the predominant current directions. The lower response time of the LOC pH sensor may have been inadvertently advantageous in this particular setting. As described above, the equilibration of the carbonate system in seawater is not complete on the timescales in this experiment. As the LOC sensor collects a volume of water before analysing it, adding a delay to the process, it can identify a larger signal than faster sensors or those not capturing fluid. A second potential weakness of this approach, specific to this demonstration, arose from the requirement to create and regularly swap two landers. Combining measurements taken by multiple instruments could be susceptible to errors due to differences between the instruments. To explore this possibility, we examined the measured pH during northbound currents (i.e. when there was no interaction with the plume) and compared these values across deployments. The mean difference between the upper and lower inlets during northbound currents was only 0.001 pH. The full data set of all measurements taken by all LOC pH sensors on both inlets and on both landers remained within a 0.031 pH unit range during northbound currents during the 12 days of measurements. This range is significantly smaller than the pH changes induced by the CO_2 release. Any differences between instruments did not have any meaningful effect on the final analysis.

Before the experiment it was uncertain whether the injection of CO_2 into the sediments would cause the expulsion of pore water from the sediments, or whether the rising bubbles would drag or push pore fluid out of the sediments as they traversed the sediment and entered the water column. The pore water in this region has TA concentrations substantially higher than found in the water column (Dale et al., 2021). In particular, the sediments directly at the ebullition points of the CO_2 bubbles had particularly high TA, up to 10 mmol/kg a few cm below the water/sediment interface(Lichtschlag et al., 2020). This effect was extremely localised and was no longer detectable a few centimetres away from the bubble ebullition points. Models designed to explore the measurements of dissolved components in the sediment suggested a very low rate of pore water ejection into the water column (Lichtschlag et al., 2020). The fact that alkalinity did not show a statistically significantly correlation with current direction suggests that there was not a detectable amount of pore water consistently entering the water column, either with the bubble stream or due to frequent disturbance of the sediment by the ROV. In either case, there would have been higher alkalinity and/or higher variance during southbound currents than during northbound currents. An identical LOC TA sensor was deployed

on a "baseline" lander, 375 m southeast of the experimental site, to measure the background characteristics of the area away from the release and related activity and this instrument's data showed a much smaller standard deviation (± 4.2 μmol/kg).

4.3. Potential other applications of this approach

While this application of a lab-on-chip sensors for measuring near-seafloor fluxes focused on a CO_2 release, this technique could be applied to measure spatial fluxes in a broad range of other environments and applications.

Benthic flux studies commonly rely on incubation chambers, either using collected samples or measuring with benthic chambers in situ. However, this approach offers limited spatial and temporal resolution. Benthic chambers typically remain in place for a short time (hours to days) and then need to be retrieved for analysis of the collected samples. The gradient flux and eddy covariance techniques can both be used for longer-term in situ benthic flux measurements. At the moment their wider applicability is limited by the availability of in situ sensors. Gradient flux typically measures a small signal and requires instruments which can perform high-precision in situ measurements over a long period. Eddy covariance can inherently perform highly sensitive flux measurements – in fact, in this field study it was able to not only unambiguously detect the CO_2 at the lowest release rate, but could even measure the background oxygen and DIC fluxes at the sediment-water interface (Koopmans et al., 2021). However, it requires high-frequency data collection (>1 Hz) and as a result only a limited number of parameters can be measured with this approach: oxygen (Berg et al., 2003), nitrate (Johnson et al., 2011), heat (Berg et al., 2016), conductivity (Crusius et al., 2008) and pH (Koopmans et al., 2021; Long et al., 2015).

LOC sensors could potentially be adapted into all of these above techniques to open new avenues for studies of benthic fluxes. LOCs could measure incubation samples directly within benthic chambers. This would overcome the requirement to collect and preserve samples for later analysis, which would allow a benthic chamber to serve as a longer-term analysis tool on, for example, a moving benthic platform. While the LOC sensors are too slow for eddy covariance, they could be used for the relaxed eddy accumulation technique in which slower concentration measurements are paired with fast velocity measurements (Lemaire et al., 2017). The gradient flux method demonstrated in the work could readily be expanded to other application areas and to use LOC sensors for other parameters. The LOC sensors described here (pH, alkalinity) are based on a platform technology which has been previously implemented and demonstrated elsewhere, for example, for nitrate (Beaton et al., 2012), phosphate (Clinton-Bailey et al., 2017; Grand et al., 2017), iron (Geißler et al., 2017) and silicate (Clinton-Bailey et al., 2019).

Measurements of fluxes with any of these sensors could be of interest in, for example, studies of metabolism of benthic environments as long as the characteristic time scales of change were comparable to the LOC sensor analysis time. This autonomous approach would also be of particular benefit in areas where ship access can be difficult, such as in areas with frequent storms, or in remote sites or polar regions, e.g. (Hoffmann et al., 2018). Since the sensors withdraw water through filters, they can also be adapted to measure pore water within sediments as well as in the water column, enabling a more complete characterisation of the benthic fluxes over the sediment-water interface. A similar approach to detecting and quantifying plumes could be implemented for other point sources or fluxes, either natural (e.g. gas seeps, hydrothermal vents) or anthropogenic (e.g. discarded waste, nutrient-rich outflows, sewage, excess aquaculture feed).

5. Conclusion

Autonomous lab-on-chip sensors were able to successfully detect and quantify a subsea CO_2 release through measurements of vertical chemical gradients. The use of novel sensors with multiple inlets allowed for a flexible setup with minimal additional hardware requirements beyond current meters. The CO_2 release could be quantified at rates an order of magnitude below a likely regulatory requirement, and at lower rates than would produce an environmental impact. This technique is both selective and sensitive enough to be a useful addition to the monitoring of offshore CO_2 reservoirs.

Declaration of Competing Interest

The authors declare the following financial interests/personal relationships which may be considered as potential competing interests: Matt Mowlem is a director, CTO, shareholder and employee of ClearWater Sensors Ltd. that manufacture and sell Lab on Chip chemical sensors utilising intellectual property licensed from the University of Southampton and the National Oceanography Centre. This IP is also used in the sensors described in this paper. Matt maintains employment in the NOC with interactions governed by a detailed conflict of interest policy. Sam Monk was a student and then postdoc at the University of Southampton and NOC during the development of sensors and the fieldwork described in the paper, but now is a visiting associate at the NOC and works is an employee of exclusively for ClearWater Sensors Ltd. The remaining authors declare that they have no known competing interests.

Acknowledgements

The authors thank the crew of the RV James Cook and of the remote-operated vehicle ISIS for making expedition JC180 such a success. We thank our colleagues at the National Oceanography Centre who played a role in the development and production of the sensor systems used here, including Urska Martincic, Anthony Kenny, Christopher Cardwell, John Walk, Hannah Wright, Alexander Beaton, Robin Brown, James Wyatt, and Kevin Saw. The authors also thank Prof. Doug Connelly and Dr. Carla Sands, the STEMM-CCS project's coordinator and project manager respectively, for their support and leadership throughout this work.

Funding sources

The STEMM-CCS project has received funding from the European Union's Horizon 2020 research and innovation programme under grant agreement No. 654462.

Other work which contributed to this experiment has been funded by the UK's Natural Environmental Research Council: the SPITFIRE project, grant number NE/L002531/1; the Climate Linked Atlantic Sector Science project, funded through the single centre national capability programme grant number NE/R015953/1; the Carbonate Chemistry Autonomous Sensor System (CarCASS) project, grant number NE/P02081X/1. The research leading to these results has received funding from the European Union Seventh Framework Programme (FP7/2007–2013) under grant agreement number 614141 (SenseOCEAN).

Further funding was received from the Max Planck Society, Germany.

References

Beaton, A.D., Cardwell, C.L., Thomas, R.S., Sieben, V.J., Legiret, F.-.E., Waugh, E.M., Statham, P.J., Mowlem, M.C., Morgan, H., 2012. Lab-on-chip measurement of nitrate and nitrite for in situ analysis of natural waters. Environ. Sci. Technol. 46, 9548–9556. https://doi.org/10.1021/es300419u.

Berg, P., Koopmans, D.J., Huettel, M., Li, H., Mori, K., Wüest, A., 2016. A new robust oxygen-temperature sensor for aquatic eddy covariance measurements. Limnol. Oceanogr. 14, 151–167. https://doi.org/10.1002/lom3.10071.

Berg, P., Røy, H., Janssen, F., Meyer, V., Jørgensen, B.B., Huettel, M., de Beer, D., 2003. Oxygen uptake by aquatic sediments measured with a novel non-invasive eddy-correlation technique. Mar. Ecol. Prog. Ser. 261, 75–83 https://doi.org/Berg, P., Røy, H., Janssen, F. ORCID: https://orcid.org/0000-0002-5607-4012 <https://orcid.org/0000-0002-5607-4012>, Meyer, V., Jørgensen, B., Huettel, M. and de Beer, D. (2003) Oxygen uptake by aquatic sediments measured with a novel non-

invasive eddy-correlation technique, Marine Ecology Progress Series, 261, pp. 75-83. doi:https://doi.org/10.3354/meps261075 <https://doi.org/10.3354/meps261075>, hdl:10013/epic.50540.

Blackford, J., Alendal, G., Avlesen, H., Brereton, A., Cazenave, P.W., Chen, B., Dewar, M., Holt, J., Phelps, J., 2020. Impact and detectability of hypothetical CCS offshore seep scenarios as an aid to storage assurance and risk assessment. Int. J. Greenhouse Gas Control 95, 102949. https://doi.org/10.1016/j.ijggc.2019.102949.

Blackford, J., Artioli, Y., Clark, J., de Mora, L., 2017. Monitoring of offshore geological carbon storage integrity: implications of natural variability in the marine system and the assessment of anomaly detection criteria. Int. J. Greenhouse Gas Control 64, 99–112. https://doi.org/10.1016/j.ijggc.2017.06.020.

Breland, J.A., Byrne, R.H., 1993. Spectrophotometric procedures for determination of sea water alkalinity using bromocresol green. Deep Sea Res. Part I 40, 629–641. https://doi.org/10.1016/0967-0637(93)90149-W.

Clinton-Bailey, G.S., Beaton, A.D., Patey, M., Davey, E., Fowell, S., Martin, A., White, S. N., Birchill, A.J., Mowlem, M.C., 2019. 'Lab-on-Chip' Sensor for in situ Determination of Silicate in Natural Waters, in: Goldschmidt Abstracts. p. 634.

Clinton-Bailey, G.S., Grand, M.M., Beaton, A.D., Nightingale, A.M., Owsianka, D.R., Slavik, G.J., Connelly, D.P., Cardwell, C.L., Mowlem, M.C., 2017. A Lab-on-Chip analyzer for in situ measurement of soluble reactive phosphate: improved phosphate blue assay and application to fluvial monitoring. Environ. Sci. Technol. 51, 9989–9995. https://doi.org/10.1021/acs.est.7b01581.

Connelly, D., 2019. JC180 cruise report - strategies for the environmental monitoring of marine carbon capture and storage. STEMM-CCS (No. JC180). RRS James Cook. Southampton, United Kingdom.

Crusius, J., Berg, P., Koopmans, D.J., Erban, L., 2008. Eddy correlation measurements of submarine groundwater discharge. Mar. Chem. 109, 77–85. https://doi.org/10.1016/j.marchem.2007.12.004.

Dale, A.W., Sommer, S., Lichtschlag, A., Koopmans, D., Haeckel, M., Kossel, E., Deusner, C., Linke, P., Scholten, J., Wallmann, K., van Erk, M.R., Gros, J., Scholz, F., Schmidt, M., 2021. Defining a biogeochemical baseline for sediments at Carbon Capture and Storage (CCS) sites: an example from the North Sea (Goldeneye). Int. J. Greenh. Gas Control 106, 103265. https://doi.org/10.1016/j.ijggc.2021.103265.

de Beer, D., Lichtschlag, A., Flohr, A., van Erk, M.R., Ahmerkamp, S., Holtappels, M., Haeckel, M., Strong, J., 2021. Sediment acidification and temperature increase in an artificial CO2 vent. Int. J. Greenh. Gas Control 105, 103244. https://doi.org/10.1016/j.ijggc.2020.103244.

Dean, M., Blackford, J., Connelly, D., Hines, R., 2020. Insights and guidance for offshore CO2 storage monitoring based on the QICS, ETI MMV, and STEMM-CCS projects. Int. J. Greenh. Gas Control 100, 103120. https://doi.org/10.1016/j.ijggc.2020.103120.

Dean, M., Tucker, O., 2017. A risk-based framework for Measurement, Monitoring and Verification (MMV) of the Goldeneye storage complex for the Peterhead CCS project, UK. Int. J. Greenh. Gas Control 61, 1–15. https://doi.org/10.1016/j.ijggc.2017.03.014.

Dewar, M., Saleem, U., Flohr, A., Schaap, A., Strong, J., Li, J., Roche, B., Bull, J., Chen, B., Blackford, J.C., 2021. Analysis of the physicochemical detectability and impacts of offshore CO2 leakage through multi-scale modelling of in-situ experimental data using the PLUME model. Int. J. Greenh. Gas Control (submitted, this issue).

Dewar, M., Sellami, N., Chen, B., 2015. Dynamics of rising CO2 bubble plumes in the QICS field experiment: part 2 – Modelling. Int. J. Greenh. Gas Control, CCS Marine Environ. 38, 52–63. https://doi.org/10.1016/j.ijggc.2014.11.003.

Dickson, A.G., Sabine, C.L., Christian, J.R., 2007. Guide to Best Practices For Ocean CO2 Measurements. (Report). North Pacific Marine Science Organization.

Esposito, M., Martínez-Cabanas, M., Connelly, D., Jasinski, D., Linke, P., Schmidt, M., Achterberg, E., 2020. Water column baseline assessment for offshore Carbon Dioxide Capture and Storage (CCS) sites: analysis of field data from the Goldeneye storage complex area. Int. J. Greenh. Gas Control (submitted, this issue).

Flohr, A., Matter, J., James, R., Saw, K., Brown, R., Ballentine, C., Day, C., Connelly, D., Flude, S., Gros, J., Hillegonds, D., Lichtschlag, A., Pearce, C., Peel, K., Strong, J., Tyne, R., 2021a. Utility of natural and artificial geochemical tracers for leakage monitoring and quantification during an offshore controlled CO2 release experiment. Int. J. Greenh. Gas Control (submitted, this issue).

Flohr, A., Schaap, A., Achterberg, E.P., Alendal, G., Arundell, M., Berndt, C., Blackford, J., Böttner, C., Borisov, S.M., Brown, R., Bull, J.M., Carter, L., Chen, B., Dale, A.W., de Beer, D., Dean, M., Deusner, C., Dewar, M., Durden, J.M., Elsen, S., Esposito, M., Faggetter, M., Fischer, J.P., Gana, A., Gros, J., Haeckel, M., Hanz, R., Holtappels, M., Hosking, B., Huvenne, V.A.I., James, R.H., Koopmans, D., Kossel, E., Leighton, T.G., Li, J., Lichtschlag, A., Linke, P., Loucaides, S., Martínez-Cabanas, M., Matter, J.M., Mesher, T., Monk, S., Mowlem, M., Oleynik, A., Papadimitriou, S., Paxton, D., Pearce, C.R., Peel, K., Roche, B., Ruhl, H.A., Saleem, U., Sands, C., Saw, K., Schmidt, M., Sommer, S., Strong, J.A., Triest, J., Ungerböck, B., Walk, J., White, P., Widdicombe, S., Wilson, R.E., Wright, H., Wyatt, J., Connelly, D., 2021b. Towards improved monitoring of offshore carbon storage: a real-world field experiment detecting a controlled sub-seafloor CO2 release. Int. J. Greenh. Gas Control 106, 103237. https://doi.org/10.1016/j.ijggc.2020.103237.

Friedlingstein, P., Jones, M.W., O'Sullivan, M., Andrew, R.M., Hauck, J., Peters, G.P., Peters, W., Pongratz, J., Sitch, S., Le Quéré, C., Bakker, D.C.E., Canadell, J.G., Ciais, P., Jackson, R.B., Anthoni, P., Barbero, L., Bastos, A., Bastrikov, V., Becker, M., Bopp, L., Buitenhuis, E., Chandra, N., Chevallier, F., Chini, L.P., Currie, K.I., Feely, R. A., Gehlen, M., Gilfillan, D., Gkritzalis, T., Goll, D.S., Gruber, N., Gutekunst, S., Harris, I., Haverd, V., Houghton, R.A., Hurtt, G., Ilyina, T., Jain, A.K., Joetzjer, E., Kaplan, J.O., Kato, E., Klein Goldewijk, K., Korsbakken, J.I., Landschützer, P., Lauvset, S.K., Lefèvre, N., Lenton, A., Lienert, S., Lombardozzi, D., Marland, G., McGuire, P.C., Melton, J.R., Metzl, N., Munro, D.R., Nabel, J.E.M.S., Nakaoka, S.-I., Neill, C., Omar, A.M., Ono, T., Peregon, A., Pierrot, D., Poulter, B., Rehder, G., Resplandy, L., Robertson, E., Rödenbeck, C., Séférian, R., Schwinger, J., Smith, N., Tans, P.P., Tian, H., Tilbrook, B., Tubiello, F.N., van der Werf, G.R., Wiltshire, A.J., Zaehle, S., 2019. Global Carbon Budget 2019. Earth Syst. Sci. Data 11, 1783–1838. https://doi.org/10.5194/essd-11-1783-2019.

Gale, J., Abanades, J.C., Bachu, S., Jenkins, C., 2015. Special Issue commemorating the 10th year anniversary of the publication of the Intergovernmental Panel on Climate Change Special Report on CO2 Capture and Storage. Int. J. Greenh. Gas Control 40, 1–5. https://doi.org/10.1016/j.ijggc.2015.06.019. Special Issue commemorating the 10th year anniversary of the publication of the Intergovernmental Panel on Climate Change Special Report on CO2 Capture and Storage.

Geißler, F., Achterberg, E.P., Beaton, A.D., Hopwood, M.J., Clarke, J.S., Mutzberg, A., Mowlem, M.C., Connelly, D.P., 2017. Evaluation of a ferrozine based autonomous in situ lab-on-chip analyzer for dissolved iron species in coastal waters. Front. Mar. Sci. 4 https://doi.org/10.3389/fmars.2017.00322.

Grand, M.M., Clinton-Bailey, G.S., Beaton, A.D., Schaap, A.M., Johengen, T.H., Tamburri, M.N., Connelly, D.P., Mowlem, M.C., Achterberg, E.P., 2017. A Lab-On-Chip Phosphate Analyzer for Long-term In Situ Monitoring At Fixed Observatories: Optimization and Performance Evaluation in Estuarine and Oligotrophic Coastal Waters. Front. Mar. Sci. 4. https://doi.org/10.3389/fmars.2017.00255.

Hoffmann, R., Braeckman, U., Hasemann, C., Wenzhöfer, F., 2018. Deep-sea benthic communities and oxygen fluxes in the Arctic Fram Strait controlled by sea-ice cover and water depth. Biogeosciences 15, 4849–4869. https://doi.org/10.5194/bg-15-4849-2018.

Holtappels, M., Kuypers, M.M.M., Schlüter, M., Brüchert, V., 2011. Measurement and interpretation of solute concentration gradients in the benthic boundary layer. Limnol. Oceanogr. 9, 1–13. https://doi.org/10.4319/lom.2011.9.1.

IEA Greenhouse Gas R&D Programme (IEA GHG), 2008. Assessment of sub sea ecosystem impacts (No. 2008/8).

IPCC, 2018. Summary for Policymakers. In: global Warming of 1.5 °C. An IPCC Special Report on the impacts of global warming of 1.5 °C above pre-industrial levels and related global greenhouse gas emission pathways, in the context of strengthening the global response to the threat of climate change, sustainable development, and efforts to eradicate poverty [Masson-Delmotte, V., P. Zhai, H.-O. Pörtner, D. Roberts, J. Skea, P.R. Shukla, A. Pirani, W. Moufouma-Okia, C. Péan, R. Pidcock, S. Connors, J. B.R. Matthews, Y. Chen, X. Zhou, M.I. Gomis, E. Lonnoy, T. Maycock, M. Tignor, and T. Waterfield (eds.)]. World Meteorological Organization, Geneva, Switzerland.

[IPCC, 2005. IPCC Special Report on Carbon Dioxide Capture and Storage. Prepared by Working Group III of the Intergovernmental Panel on Climate Change,]. In: Metz, B., Davidson, O., de Coninck, H.C., Loos, M., Meyer, L.A. (Eds.), World Meteorological Organization, eds. Cambridge University Press, Cambridge, United Kingdom and New York, NY, USA.

Johnson, K.S., Barry, J.P., Coletti, L.J., Fitzwater, S.E., Jannasch, H.W., Lovera, C.F., 2011. Nitrate and oxygen flux across the sediment-water interface observed by eddy correlation measurements on the open continental shelf. Limnol. Oceanogr. 9, 543–553. https://doi.org/10.4319/lom.2011.9.543.

Kita, J., Stahl, H., Hayashi, M., Green, T., Watanabe, Y., Widdicombe, S., 2015. Benthic megafauna and CO2 bubble dynamics observed by underwater photography during a controlled sub-seabed release of CO2. Int. J. Greenh. Gas Control, CCS Mar. Environ. 38, 202–209. https://doi.org/10.1016/j.ijggc.2014.11.012.

Koopmans, D., Meyer, V., Holtappels, M., Schaap, A., Dewar, M., Färber, P., Long, M.H., Connelly, D., de Beer, D., 2021. Detection and quantification of a release of carbon dioxide gas from the seafloor using pH eddy covariance and measurements of plume advection. Int. J. Greenh. Gas Control (submitted, this issue).

Lemaire, B.J., Noss, C., Lorke, A., 2017. Toward relaxed eddy accumulation measurements of sediment-water exchange in aquatic ecosystems. Geophys. Res. Lett. 44, 8901–8909. https://doi.org/10.1002/2017GL074625.

Lewis, E., Wallace, D.W.R., 1998. Program Developed for CO2 System Calculations. ORNL/CDIAC-105, Carbon Dioxide Inf. Anal. Cent., Oak Ridge Natl. Lab., Oak Ridge, Tenn., 38 pp., https://salish-sea.pnnl.gov/media/ORNL-CDIAC-105.pdf.

Li, J., White, P.R., Roche, B., Bull, J.M., Leighton, T.G., Davis, J.W., Fone, J.W., 2021. Acoustic and optical determination of bubble size distributions – Quantification of seabed gas emissions. Int. J. Greenh. Gas Control 108, 103313. https://doi.org/10.1016/j.ijggc.2021.103313.

Li, Q., Wang, F., Wang, Z.A., Yuan, D., Dai, M., Chen, J., Dai, J., Hoering, K.A., 2013. Automated Spectrophotometric Analyzer for Rapid Single-Point Titration of Seawater Total Alkalinity. Environ. Sci. Technol. 47, 11139–11146. https://doi.org/10.1021/es402421a.

Lichtschlag, A., Blackford, J.C., Borisov, S., Bull, J., de Beer, D., Dean, M., Flohr, A., Esposito, M., Gros, J., Haeckel, M., Huvenne, V., James, R., Linke, P., Mowlem, M., Koopmans, D., Omar, A., Pearce, C., Schaap, A., Schmidt, M., Sommer, S., Strong, J., Suominen, M., Connelly, D., 2021. Suitability analysis and revised strategies for marine environmental carbon capture and storage (CCS) monitoring. Int. J. Greenh. Gas Control submitted, this issue.

Lichtschlag, A., Haeckel, M., Olierook, D., Peel, K., Flohr, A., Pearce, C., James, R., Marieni, C., Connelly, D., 2020. Impact of CO2 leakage from sub-seabed carbon dioxide capture and storage on the geochemistry of sediments. Int. J. Greenh. Gas Control submitted, this issue.

Long, M.H., Charette, M.A., Martin, W.R., McCorkle, D.C., 2015. Oxygen metabolism and pH in coastal ecosystems: eddy Covariance Hydrogen ion and Oxygen Exchange System (ECHOES). Limnol. Oceanogr. 13, 438–450. https://doi.org/10.1002/lom3.10038.

Mabon, L., Shackley, S., Blackford, J.C., Stahl, H., Miller, A., 2015. Local perceptions of the QICS experimental offshore CO2 release: results from social science research. Int. J. Greenh. Gas Control, CCS Mar. Environ. 38, 18–25. https://doi.org/10.1016/j.ijggc.2014.10.022.

McGillis, W.R., Langdon, C., Loose, B., Yates, K.K., Corredor, J., 2011. Productivity of a coral reef using boundary layer and enclosure methods. Geophys. Res. Lett. 38 https://doi.org/10.1029/2010GL046179.

Monk, S., Schaap, A., Hanz, R., Borisov, S., Loucaides, S., Arundell, M., Papadimitriou, S., Walk, J., Tong, D., Wyatt, J., Mowlem, M., 2021. Detecting and mapping a CO2 plume with novel autonomous sensors on an underwater remote-operated vehicle. Int. J. Greenh. Gas Control submitted, this issue.

Omar, A.M., García-Ibáñez, M.I., Schaap, A., Oleynik, A., Esposito, M., Jeansson, E., Loucaides, S., Thomas, H., Alendal, G., 2021. Detection and quantification of CO2 seepage in seawater using the stoichiometric Cseep method: results from a recent subsea CO2 release experiment in the North Sea. Int. J. Greenh. Gas Control 108, 103310. https://doi.org/10.1016/j.ijggc.2021.103310.

Rérolle, V.M.C., Floquet, C.F.A., Harris, A.J.K., Mowlem, M.C., Bellerby, R.R.G.J., Achterberg, E.P., 2013. Development of a colorimetric microfluidic pH sensor for autonomous seawater measurements. Anal. Chim. Acta 786, 124–131. https://doi.org/10.1016/j.aca.2013.05.008.

Roche, B., Bull, J., Marin-Moreno, H., Leighton, T., Falcon-Suarez, I., White, P., Provenzano, G., Tholen, M., Li, J., Faggetter, M., 2021. Time-lapse imaging of CO2 migration within near-surface sediments during a controlled sub-seabed release experiment. Int. J. Greenh. Gas Control submitted, this issue.

Royal Society, 2005. Ocean Acidification Due to Increasing Atmospheric Carbon Dioxide. The Royal Society, London.

Schmidt, M., 2019. RV POSEIDON Fahrtbericht /Cruise Report POS534 STEMM-CCS: strategies for Environmental Monitoring of Marine Carbon Capture and Storage Leg 1: Kiel (Germany) - Aberdeen (United Kingdom) 01.05 - 22.05.2019 Leg 2: Aberdeen (United Kingdom) - Bremerhaven (Germany) 23.05 - 29.05.2019 (No. 2193–8113). GEOMAR Helmholtz-Zentrum für Ozeanforschung, Kiel, Germany.

Schulz, K.G., Riebesell, U., Rost, B., Thoms, S., Zeebe, R.E., 2006. Determination of the rate constants for the carbon dioxide to bicarbonate inter-conversion in pH-buffered seawater systems. Mar. Chem. 100, 53–65. https://doi.org/10.1016/j.marchem.2005.11.001.

Staudinger, C., Strobl, M., Fischer, J.P., Thar, R., Mayr, T., Aigner, D., Müller, B.J., Müller, B., Lehner, P., Mistlberger, G., Fritzsche, E., Ehgartner, J., Zach, P.W., Clarke, J.S., Geißler, F., Mutzberg, A., Müller, J.D., Achterberg, E.P., Borisov, S.M., Klimant, I., 2018. A versatile optode system for oxygen, carbon dioxide, and pH measurements in seawater with integrated battery and logger. Limnol. Oceanogr. 16, 459–473. https://doi.org/10.1002/lom3.10260.

Takeshita, Y., McGillis, W., Briggs, E.M., Carter, A.L., Donham, E.M., Martz, T.R., Price, N.N., Smith, J.E., 2016. Assessment of net community production and calcification of a coral reef using a boundary layer approach. J. Geophys. Res. 121, 5655–5671. https://doi.org/10.1002/2016JC011886.

van Heuven, S., Pierrot, D., Rae, J.W.B., Lewis, E., Wallace, D.W.R., 2011. MATLAB Program Developed For CO2 System Calculations. ORNL/CDIAC-105b. Carbon Dioxide Information Analysis Center. Oak Ridge National Laboratory, U.S. Department of Energy, Oak Ridge, Tennessee.

Vielstädte, L., Linke, P., Schmidt, M., Sommer, S., Haeckel, M., Braack, M., Wallmann, K., 2019. Footprint and detectability of a well leaking CO2 in the Central North Sea: implications from a field experiment and numerical modelling. Int. J. Greenh. Gas Control 84, 190–203. https://doi.org/10.1016/j.ijggc.2019.03.012.

Wang, Z.A., Moustahfid, H., Mueller, A.V., Michel, A.P.M., Mowlem, M., Glazer, B.T., Mooney, T.A., Michaels, W., McQuillan, J.S., Robidart, J.C., Churchill, J., Sourisseau, M., Daniel, A., Schaap, A., Monk, S., Friedman, K., Brehmer, P., 2019. Advancing Observation of Ocean Biogeochemistry, Biology, and Ecosystems With Cost-Effective in situ Sensing Technologies. Front. Mar. Sci. 6 https://doi.org/10.3389/fmars.2019.00519.

Yin, T., Papadimitriou, S., Rérolle, V., Arundell, M., Cardwell, C.L., Walk, J., Palmer, M., Fowell, S., Schaap, A., Mowlem, M., Loucaides, S., 2021. A Novel Lab-On-Chip Spectrophotometric pH Sensor For Autonomous in Situ Seawater Measurements to 6000 m Depth On Stationary and Moving Observing Platforms. In review.